Emildo Marcano[1]

DFT study of anthocyanidin and anthocyanin pigments for Dye-Sensitized Solar Cells: Electron injecting from the excited states and adsorption onto TiO_2 (anatase) surface

[1] Instituto Pedagógico de Caracas, Centro de Investigaciones en Ciencias Naturales (CICNAT), Laboratorio de Química Computacional, Universidad Pedagógica Experimental Libertador, Apartado 47102, Caracas 1020-A, E-mail: jedi148@gmail.com

Abstract:
We explored, the absorption spectra, excited states and electronic injection parameters of anthocyanidin and anthocyanin pigments using the level of theory (TD)CAM-B3LYP/6-31+G(d,p). For the most isolated dyes, the distribution pattern of HOMO and LUMO spreads over the whole molecules, which lead an efficient electronic delocalization. The calculated light harvesting efficiencies (LHEs) are all near unity. Methoxy group in peonidin molecule lead the largest oscillator strength and LHE. The presence of water lead a higher spontaneous electronic inject process, with ΔG_{inject} average of –1.14 eV. The ΔG_{inject} order is peonidin < delphinidin < cyanin < cyanidin. Similarly, the adsorption energies (E_{ads}) onto anatase surface model were obtained from level of theory GGA(PBE)/DNP. E_{ads} of anthocyanin–$(TiO_2)_{30}$ complex was calculated to be from 17 to 24 eV, indicating both, the strong interactions between the dyes and the anatase (TiO_2) surface and stronger electronic coupling strengths of the anthocyanin–$(TiO_2)_{30}$ complex, which corresponded to higher observed η. The HOMO and LUMO shape showed the electrons delocalized predominantly on the anthocyanin structure while the LUMO + 1 shape is localized into the $(TiO_2)_{30}$ surface. Therefore, we expected a electronic injection from HOMO to LUMO + 1 in the anthocyanin–$(TiO_2)_{30}$ adsorption complex, after the light absorption.

Keywords: anthocyanin, anatase (TiO_2) surface, adsorption energies, electronic injection
DOI: 10.1515/psr-2017-0008

1 Introduction

Dye-sensitized solar cells (DSSC) based on organic dyes adsorbed on nanocrystalline TiO_2 electrodes have attracted considerable attention in recent years because of their high incident solar light → electricity conversion efficiency and low cost of production [1, 2]. The driving force in these is the interfacial electron injection from the dye to the semiconductor. Upon absorbing light, the dye molecules are excited from their ground state, which is located energetically in the semiconductor band gap, to an excited state that is resonant with the TiO_2 conduction band. The electron is then transferred to the semiconductor on the ultrafast time scale [3]. The relative yields and rates of electron injection, recombination, and decay of the dye-excited state influence the efficiency of the solar cell [4]. Therefore, improving the efficiency of the solar devices is possible only when the rates and mechanisms of the competing reactions are known and understood. This in turn requires knowledge of the electronic structure of the dyes both, before and after binding to the semiconductor surface [5]. The photochemical properties of different organic sensitizers have extensively been investigated in an attempt to design dyes with maximal visible light absorption coupled to long-lived excited states. However, major effort is still needed in both developing new sensitizers and finding optimal working conditions to improve the photon → current conversion efficiencies [6–8]. In this framework, natural dyes as photosensitizers for DSSCs are very attractive because they are of low cost, abundant in supply and sustainable [9]-[12]. Specifically, several types of natural dyes belonging to anthocyanin have been performed. The anthocyanins belong to the group of natural dyes responsible for several colors in red-blue range, found in fruits, flower and leaves of plants. The dyes extracted from grape, mulberry, blackberry, red Sicilian orange, Sicilian prickly pear, eggplant and radicchio have shown a monochromatic incident photon to current efficiency (IPCE) ranging from 40 % to 69 %. Short circuit photocurrent densities (J_{sc}) up to 8.8 mA/cm^2, open circuit voltage (V_{oc}) ranging from 316 to 419

Emildo Marcano is the corresponding author.

mV and solar conversion efficiency of 2.06 % [13–15]. Despite several experimental results about the performance of anthocyanin pigments in DSSC, there are no systematic calculations of their electron transference mechanism from the excited states and adsorption onto TiO_2 surface to the best of our knowledge. Within this framework, the main objectives of this paper are to explore, using theoretical calculations, the electronic properties of anthocyanidin and anthocyanin pigments after and before adsorption onto TiO_2 (anatase) surface. The characterization of electronic properties for dyes in gas phase was carried out using the level of theory CAM-B3LYP, employing the 6-31+G(d,p) basis set. The absorption spectra, excited states and electronic injection parameters were obtained and analyzed at TD(CAM-B3LYP)/6-31+G(d,p). Finally, the adsorption energies onto anatase surface model were obtained and analyzed at density functional theory (DFT) level using generalized gradient-corrected approximation (GGA)(Perdew–Burke–Ernzerhof [PBE]) functional and double numerical basis set with polarization (DNP).

2 Theory and computational details

The sunlight-to-electricity conversion efficiency (η) of solar cell devices is determined by open-circuit photovoltage (V_{OC}), short-circuit current density (J_{SC}) and the fill factor (FF), as compared to incident solar power (P_{inc}) [1, 16, 17]:

$$\eta = FF\frac{V_{OC}J_{SC}}{P_{inc}} \tag{1}$$

J_{SC} is determined by the following equation:

$$J_{SC} = \int LHE(\lambda)\Phi_{inject}n_{collect}\,d\lambda \tag{2}$$

where $\eta_{collect}$ is the charge collection efficiency, for the same DSSCs differing only in the dye. As is the case for the organic dyes under study, it is reasonable to assume that this parameter is constant. Light harvesting efficiency (LHE (λ) is the fraction of the incident photons that are absorbed by the dye. LHE is related to the oscillator strength (f) at a given wavelength. By the following equation, while the larger f, the stronger LHE [18]:

$$LHE = 1 - 10^{-f} \tag{3}$$

The Φ_{inject} parameter evinces the electron injection efficiency and is related to the driving force ΔG_{inject} of electrons injecting from the excited states of dye molecules to the semiconductor substrate. It can be estimated as [19]:

$$\Delta G_{inject} = E_{OX}^{dye^*} - E_{CB}^{TiO_2} \tag{4}$$

$E_{OX}^{dye^*}$ is the excited state oxidation potential of the dye. $E_{CB}^{TiO_2}$ is the energy conduction band of the TiO_2 semiconductor (–4 eV). $E_{OX}^{dye^*}$ can be determined using following formula:

$$E_{OX}^{dye^*} = E_{OX}^{dye} - \lambda_{max}^{ICT} \tag{5}$$

In eq. 5) λ_{max}^{ICT} is the energy of intermolecular charge transfer (ICT).

DFT and time-dependent density functional theory (TDDFT) calculations were performed to determine geometries, electronic structures and electronic absorption spectra of anthocyanin dyes. All the calculations, in gas phase, were performed using GAMESS package [20]. All calculations were performed by employing CAM-B3LYP/6-31+G(d,p). On the basis of eqs 3, 4, 5), we calculated LHE and ΔG_{inject} parameters and analyzed the efficiency of anthocyanin dyes for electron injection from dye's excited state to TiO_2 (anatase) surface [21, 22].

The adsorption of dyes on the anatase cluster was performed with DFT calculations using DMol^3 program [23]. The model employed herein to represent the (100) surface of anatase consists of 30 TiO_2 units, terminated with 12 hydrogen atoms, which modeled a TiO_2 nanoparticle [24]. The initial structure has been taken from the crystal of TiO_2 anatase [25]. This model has a diameter of about 1 nm, that has to be compared to nanoparticles of about 2–6 nm used in experiments, and has been used in theoretical study of electronic absorption spectrum of organic compound supported on TiO_2, with application in DSSC [3].

The $(TiO_2)_{30}$ configurations were fully optimized using the GGA. The PBE functional was used to account exchange–correlation effects with DNP basis set. The core electron was treated with DFT-semicore pseudopotentials (DSPPs). After optimization, the adsorption energies (E_{ads}) on the $(TiO_2)_{30}$ cluster were obtained. The latter value was obtained using the equation:

$$E_{ads} = E_{TiO_2} + E_{Anth} - E_{TiO_2+Anth} \tag{6}$$

where E_{TiO_2+AmA} is the total energy of anthocyanin–$(TiO_2)_{30}$ complex, E_{TiO_2} is the energy for the anatase surface model and E_{Anth} is the energy for the anthocyanin molecule [26]. Following the above expression, a positive value of E_{ads} indicated a stable adsorption.

3 Results and discussion

3.1 Geometric optimization and intramolecular charge transferences of anthocyanin dyes

The anthocyanin chromophores molecule (cyaniding, delphinidin, peonidin and cyanin) used to carry out the calculations are displayed in Figure Figure 1. They have a positive charge on the molecule, which enables it to absorb light and thus have color [13]. As observed in Figure Figure 1, cyanidin and delphinidin differ in the number of hydroxyl groups present in the molecule, while peonidin has a substituted –OH group. Cyanin has a glucoside group. From level of theory CAM-B3LYP/6-31+G(d,p) all structures showed a planar geometric, which facilitates the electronic delocalization in all the structure. The glucoside group in cyanine dye led a small deviation in the torsion angle for the [C3-C2-C1´- C2´] bond (14°).

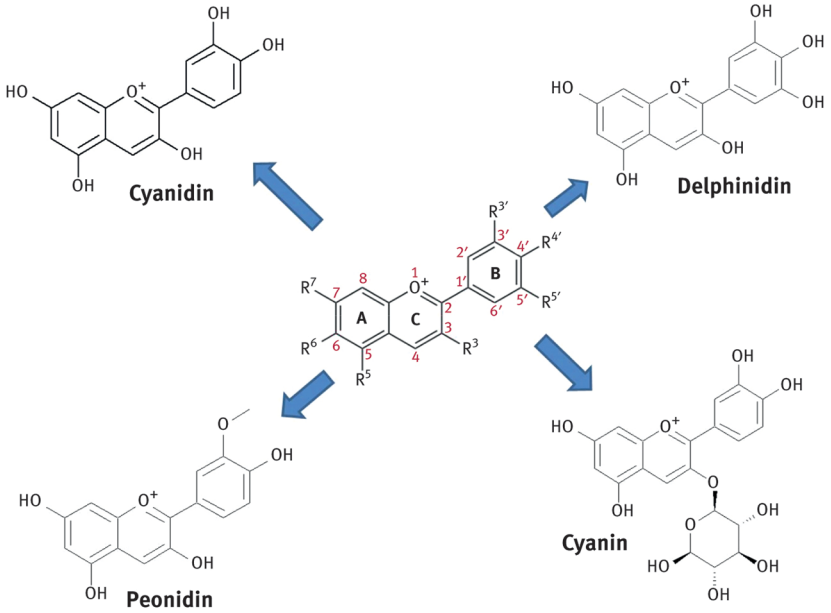

Figure 1: Anthocyanin chromophores molecules (cyanidin, delphinidin, peonidin and cyanin) studied in this work.

3.2 Frontier molecular orbitals, absorption spectra and LHE

The ground state first singlet excited state excitation process can be mainly assigned to the HOMO–LUMO transition, which correspond to a π-π* excited singlet state. For the sake of characterizing electronic properties, it is useful to examine the distribution patterns of molecular orbitals [27, 28]. On the other hand, an important thermodynamic requirement of the dyes to be used in DSSC technology is that the HOMO level of the sensitizer has to be sufficiently positive in the redox potential for efficient regeneration of the oxidized dye molecule to its original state by the iodide electrolyte and the LUMO energy of the dye has to be sufficiently higher than the conduction band edge of the semiconductor (E_{CB}). To demonstrate their characteristic electronic structure, the HOMO–LUMO shape from the anthocyanin molecules at CAM-B3LYP/6-31+G(d,p) methods in gas phase, are shown in Figure Figure 2, and the energy parameter, including solvent (water) effects with IEFPCM model, are shown in Table Table 1. With exception of cyanin, the distribution pattern of HOMO and LUMO spreads over

the whole molecule, as expected, in both, gas phase and water, which lead an efficient electronic delocalization [13]. In fact, the electronic density is shifted from the catechol moiety in ring B to the benzopyran system (ring A and C) (see Figure Figure 1). Independently of the substituted groups, in gas phase, the energy values for the HOMO and LUMO orbitals are close to the average –10.46 eV and –5.65 eV, respectively, in agreement with others reports [29], which underestimate the value corresponding to the conduction band of the anatase (–4 eV). When the effects of solvent are account, these values are increased up to –7 eV < –4 eV < –2 eV range [30]. Therefore, the LUMO energy is sufficiently higher than the conduction band edge of TiO_2, and HOMO level is lower than the redox potential of I^-/I_3^- electrolyte to regenerate the oxidized dye (–4,6 eV) [31, 32].

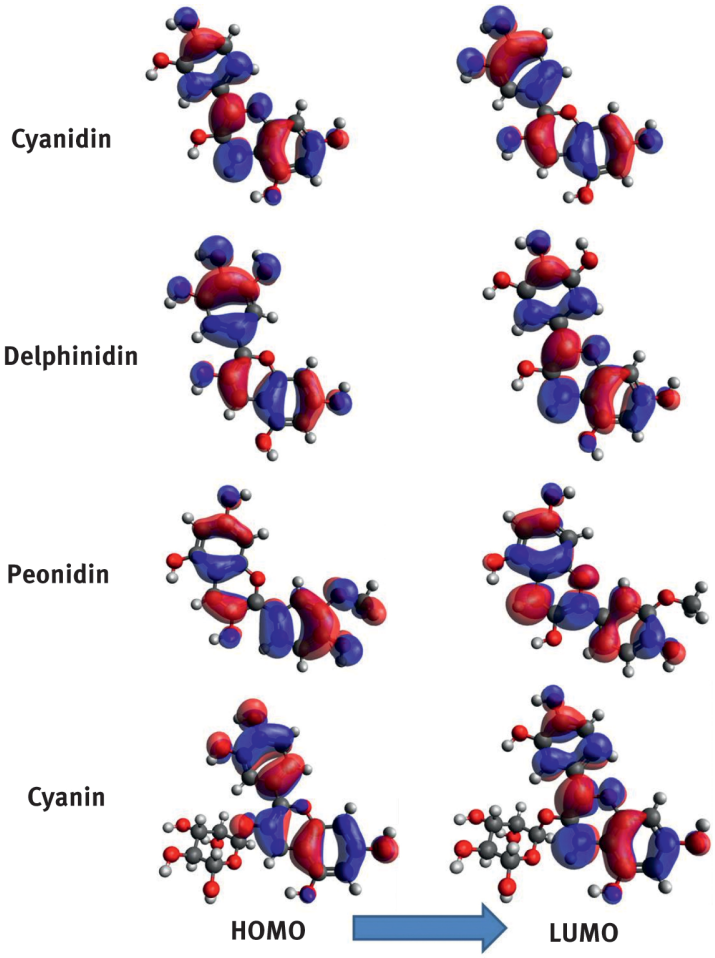

Figure 2: HOMO–LUMO shape from the anthocyanin molecules at CAM-B3LYP/6-31+G(d,p) theory level in gas phase.

Table 1: Computed HOMO, LUMO and energy gap (eV) in the gas phase and water at CAM-B3LYP/6-31+G(d,p) level.

	Gas phase			Water		
Molecule	E_{HOMO}	E_{LUMO}	E_{gap}	E_{HOMO}	E_{LUMO}	E_{gap}
Cyanidin	–10.5803	–5.7686	4.8117	–5.6660	–2.6172	5.0489
Delphinidin	–10.4320	–5.6154	4.8166	–5.6405	–2.5796	5.0608
Peonidin	–10.3659	–5.6734	4.6925	–5.6008	–2.6107	4.9901
Cyanin	–10.4992	–5.5578	4.9414	–5.7030	–2.5908	5.1122
Average	–10.4693	–5.6538	4.8156	–5.6526	–2.5996	5.0530

The calculations of the wavelength of maximum absorption (λ_{max}) and others spectroscopic parameter in water are shown in Table Table 2 at TD(CAM-B3LYP)/6-31+G(d,p). Absorption spectra for anthocyanin molecules in gas phase and water are shown in Figure Figure 3. The prediction of absorption spectra for structures studied lead two maximum wavelength in 200 nm–250 nm range, and 400 nm–450 nm range, as expected [30, 32, 33]. The λ_{max} values associated with the intramolecular charge transference (ICT), and HOMO → LUMO transition, is in the order cyanidin (446 nm) > peonidin (445 nm) > delphinidin (442 nm) > cyanin (438 nm). From delphinidin molecule, the lack of a hydroxyl group lead a two extra maximum wavelength, associated

with the transitions HOMO-4 → LUMO (229 nm) and HOMO → LUMO+2 (205 nm). Similarly, the substitution of a glucoside group in cyanin structure, lead a two extra maximum wavelength, associated with the transitions HOMO → LUMO+1 (250 nm) and HOMO-1 → LUMO+1 (237 nm).

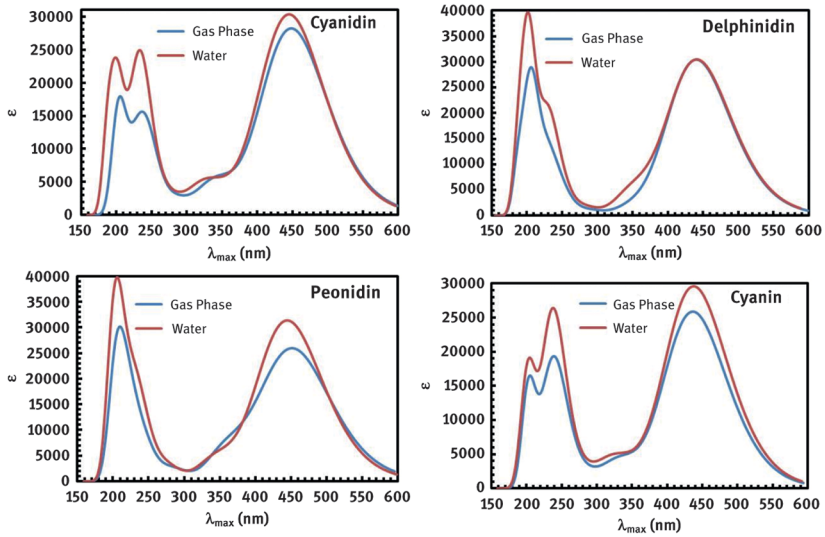

Figure 3: Absorption spectra for anthocyanin molecules in gas phase and water at TD(CAM-B3LYP)/6-31+G(d,p) theory level.

Table 2: Wavelength of maximal absorption (λ_{max}/nm), excitation energies (E_e/eV, in water, TD(CAM-B3LYP)/6-31+G(d) level), electronic transition configurations (Assignment), oscillator strengths (f) ($f > 0.1$) and LHE for anthocyanin dyes.

Molecule	λ_{max}	Assignment	Ee	f	LHE
	446.2	HOMO → LUMO (0.68)	2.78	0.742	0.8187
Cyanidin	229.2	HOMO-4 → LUMO (0.56)	5.41	0.244	
	205.6	HOMO → LUMO+2 (0.49)	6.03	0.283	
	442.2	HOMO → LUMO (0.67)	2.80	0.744	0.8198
Delphinidin	228.4	HOMO-2 → LUMO+1 (0.37)	5.43	0.321	
	206.2	HOMO → LUMO+3 (0.46)	6.01	0.322	
	445.7	HOMO → LUMO (0.66)	2.78	0.767	0.8290
Peonidin	228.4	HOMO-2 → LUMO+1 (0.36)	5.43	0.309	
	207.1	HOMO → LUMO+2 (0.36)	5.99	0.437	
	438.7	HOMO → LUMO (0.68)	2.83	0.723	0.8107
Cyanin	250.8	HOMO → LUMO+1 (0.63)	4.94	0.264	
	237.6	HOMO-1 → LUMO+1 (0.37)	5.22	0.264	

According to the eqs 1 and 2), LHE is one of the key factors in DSSC. It represents the fraction of the incident photons that are absorbed by the dye. The LHE of the dye should be as high as feasible to maximize the photo-current response. As observed in Table Table 2, the calculated LHEs are all near unity. Methoxy group in peonidin molecule lead the largest oscillator strength and LHE. On the other hand, from delphinidin molecule, the lacks of a hydroxyl group lead a decreased in the LHE. Similarly, when a glucoside group is substituted in cyanin structure, a decreased in the LHE value is found.

3.3 Free Energy Change of Electron Injection

On the basis of the knowledge of isolated dyes, we extend to study the driving force ΔG_{inject} of electrons injecting from the excited states of anthocyanin dye to the TiO_2 semiconductor substrate to analyze other factors affecting the energy conversion efficiency. Therefore, we have used eqs 4 and 5 to estimate the anthocyanin's excited state oxidation potential and free energy change of electron injection to titanium dioxide TiO_2 surface, in gas phase and water from level of theory TD(CAM-B3LYP)/6-31+G(d,p). E_{OX}^{dye} had been estimated as negative E_{HOMO} [34]. The results are show in Table Table 3. The solvent effects were evidenced in the E_{HOMO} results, which lead a significant decreased in ΔG_{inject}. Therefore, in gas phase, ΔG_{inject} have an average of 3.66 eV, while the water presence lead a higher spontaneous electronic inject process, with ΔG_{inject} average of –1.14 eV. The negative ΔG_{inject} is an indication of spontaneous electron injection from the dye to TiO_2. For the anthocyanin molecules studied, the ΔG_{inject} order is peonidin < delphinidin < cyanin < cyanidin.

Table 3: Anthocyanin's excited state oxidation potential and free energy change of electron injection to titanium dioxide TiO_2 surface, in gas phase and water at TD(CAM-B3LYP)/6-31+G(d,p) theory level.

	Gas phase				Water			
Molecule	$E^{dye}{}_{OX}$	$\lambda^{ICT}{}_{max}$	$E^{dye*}{}_{OX}$	ΔG_{inject}	$E^{dye}{}_{OX}$	$\lambda^{ICT}{}_{max}$	$E^{dye*}{}_{OX}$	ΔG_{inject}
Cyanidin	10.4320	2.7579	7.6741	3.6741	5.6660	2.7784	2.8876	–1.1124
Delphinidin	10.3659	2.8091	7.5568	3.5568	5.6405	2.8036	2.8369	–1.1631
Peonidin	10.4992	2.7204	7.7788	3.7788	5.6008	2.7820	2.8188	–1.1812
Cyanin	10.4693	2.8316	7.6377	3.6377	5.7030	2.8261	2.8769	–1.1231
Average	10.4416	2.7798	7.6619	3.6619	5.6526	2.7975	2.8551	–1.1449

3.4 Chemisorption on TiO_2-anatase

Tetragonal structure of anatase may be described using two cell edge parameters, *a* and *c*, and one internal parameter, *d* (the length of the Ti−O apical bond) [34]. In this paper, the $(TiO_2)_{30}$ configurations were optimized using the GGA. The results for the geometric parameters described before were *a* = 3.566 Å, *c* = 10.707 Å and *d* = 1.899 Å, which were comparable with experimental values (*a* = 3.782 Å, *c* = 9.502 Å, *d* = 1.979 Å) and others theoretical DFT methodology, where cluster approach methodology had been used [34–36].

In dye-TiO_2 adsorption, the adsorption of dyes through terminal –H atom can be either physisorption (via hydrogen bonding between an oxygen atom on TiO_2 surface and a hydrogen atom of the dye) or chemisorption (an H atom dissociates and the bond is formed between oxygen atoms and the surface titanium atoms of TiO_2). In this paper, we have chosen the second option. The adsorption complex was first fully optimized using the PBE functional together with the double-numerical with polarization performed in the $DMol^3$ program. The optimized structures of anthocyanin–$(TiO_2)_{30}$ adsorption complexes are show in Figure Figure 4 and the important optimized bond length and adsorption energy (E_{ads}) are listed in Table Table 4. The bond distances between Ti and O atom of dyes were calculated to be in the range of 1.89–1.97 Å. The adsorption energy (E_{ads}) of anthocyanin–$(TiO_2)_{30}$ complex was calculated to be from 17 to 24 eV, indicating the strong interactions between the dyes and the anatase (TiO_2) surface. Table Table 4 shows that a systematic change in the sunlight-to-electricity conversion efficiency (η) was observed as predicted from adsorption energies. Therefore, the higher adsorption energy resulted in the stronger electronic coupling strengths of the anthocyanin–$(TiO_2)_{30}$ complex, which corresponded to higher observed η as expected [37, 38].

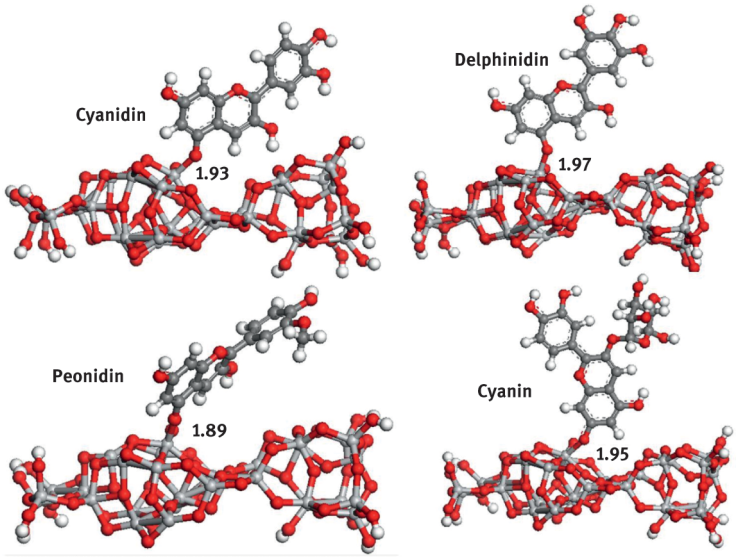

Figure 4: Optimized structures of anthocyanin–$(TiO_2)_{30}$ adsorption complexes at PBE/DNP theory level. Important optimized bond length are shown in Å.

Table 4: Important optimized bond length Ti-O (Å), adsorption energy (E_{ads}/eV) and sunlight-to-electricity conversion efficiency, η(%) for anthocyanin–$(TiO_2)_{30}$ adsorption complexes.

Molecule	Ti-O	E_{ads}	η (%)
Cyanidin	1.93	17.624	0.37
Delphinidin	1.97	18.749	0.56
Peonidin	1.89	17.889	0.62
Cyanin	1.95	24.107	0.66

In order to explore the possible intramolecular charge transference between anthocyanin dyes and anatase surface, HOMO and LUMO shape were examined by the DFT (PBE) calculations with DNP basis set. Numerical basis set was used because of its reasonable computational cost. Figure Figure 5 shows the frontier molecular orbitals of anthocyanin–$(TiO_2)_{30}$ adsorption complex in vacuum. The HOMO and LUMO shape showed the electrons delocalized predominantly on the anthocyanin structure while the LUMO + 1 shape is localized into the $(TiO_2)_{30}$ surface. Therefore we expected an electronic injection from HOMO to LUMO + 1 in the anthocyanin–$(TiO_2)_{30}$ adsorption complex, after the light absorption.

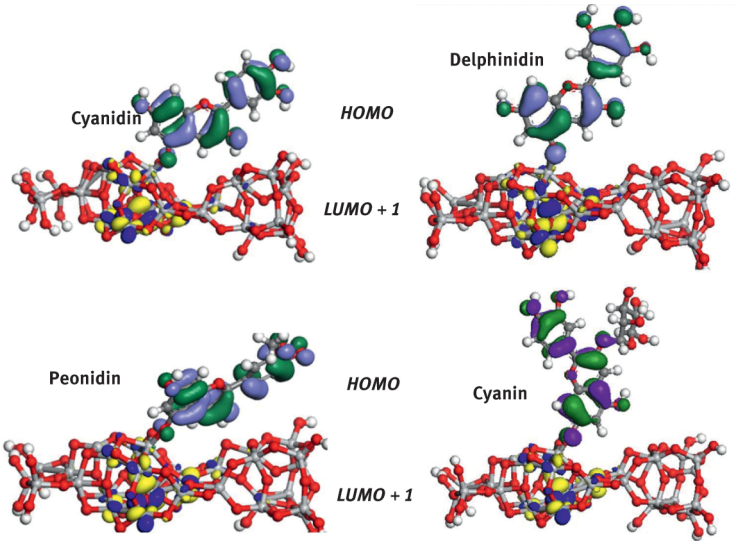

Figure 5: The HOMO (blue/green) and LUMO + 1 (blue/yellow) shapes of anthocyanin–$(TiO_2)_{30}$ adsorption complexes at PBE/DNP theory level.

Conclusions

We explored the electronic properties of anthocyanidin and anthocyanin pigments after and before adsorption onto TiO_2 (anatase) surface. The characterization of electronic properties for dyes in gas phase and water was carried out using CAM-B3LYP/6-31+G(d,p) methods. The absorption spectra, excited states and electronic injection parameters were obtained and analyzed at TD(CAM-B3LYP)/6-31+G(d,p). The adsorption energies onto anatase surface model were obtained and analyzed at DFT level using GGA(PBE) functional and numerical DNP basis set. For all isolated dyes, the distribution pattern of HOMO and LUMO spreads over the whole molecule, as expected, in both, gas phase and water, which lead an efficient electronic delocalization. The LUMO energy is sufficiently higher than the conduction band edge of TiO_2, and HOMO level is lower than the redox potential of I^-/I_3^- electrolyte to regenerate the oxidized dye. The calculated LHEs are all near unity. Methoxy group in peonidin molecule lead the largest oscillator strength and LHE. The water presence lead a higher spontaneous electronic inject process, with ΔG_{inject} average of –1.14 eV. The negative ΔG_{inject} is an indication of spontaneous electron injection from the dye to TiO_2. For the anthocyanin molecules studied, the ΔG_{inject} order is peonidin < delphinidin < cyanin < cyanidin. The adsorption energy (E_{ads}) of anthocyanin–$(TiO_2)_{30}$ complex was calculated to be from 17 to 24 kcal/mol, indicating the strong interactions between the dyes and the anatase (TiO_2) surface. Therefore, the higher adsorption energy resulted in the stronger electronic coupling strengths of the anthocyanin–$(TiO_2)_{30}$ complex, which corresponded to higher observed η as expected. The HOMO and LUMO shape showed the electrons delocalized predominantly on the anthocyanin structure while the LUMO + 1 shape is localized into the $(TiO_2)_{30}$ surface. Therefore we expected an electronic injection from HOMO to LUMO + 1 in the anthocyanin–$(TiO_2)_{30}$ adsorption complex, after the light absorption.

Acknowledgments

The author, Emildo Marcano, acknowledge support by Fondo Nacional de Ciencia, Tecnología e Innovación (FONACIT) through grant PEI-1852.

This article is also available in: Ramasami, Computational Sciences. De Gruyter (2017), isbn 978-3-11-046536-5.

References

[1] Hagfeldt A, Boschloo G, Sun L, Kloo L, Pettersson H. Dye-sensitized solar cells. Chem Rev. 2010;110:6595–6663.
[2] Vittadini A, Casarin M, Selloni A. Chemistry of and on TiO_2-anatase surfaces by DFT calculations: A partial review. Theor Chem Acc. 2007;117:663–671.
[3] Sánchez De Armas R, Oviedo López J, San Miguel MA. Real-time TD-DFT simulations in dye sensitized solar cells: The electronic absorption spectrum of alizarin supported on TiO_2 nanoclusters. J Chem Theory Comput. 2010;6:2856–2865.
[4] Xie M, Bai FQ, Wang J, Kong CP, Chen J, Zhang HX. Theoretical description of dye regeneration on the TiO_2–dye–electrolyte model. Comput Mater Sci. 2016;111:239–246.
[5] Duncan WR, Prezhdo OV. Electronic structure and spectra of catechol and alizarin in the gas phase and attached to titanium. J Phys Chem B. 2005;109:365–373.
[6] Manzhos S, Giorgi G, Yamashita K. A density functional tight binding study of acetic acid adsorption on crystalline and amorphous surfaces of titania. Molecules. 2015;20:3371–3388.
[7] Jungsuttiwong S, Tarsang R, Surakhot Y, Khunchalee J, Sudyoadsuk T, Promarak V, et al. Theoretical study of α-fluorenyl oligothiophenes as color tunable emissive materials for highly efficient electroluminescent device. Org Electron. 2012;13:1836–1843.
[8] Zhu C, Liang J, Cao Z. Unique metal dicorrole dyes with excellent photoelectronic properties for solar cells: Insight from density functional calculations. J Phys Chem C. 2013;117 13388—13395.
[9] Gao FG, Bard AJ, Kispert LD. Photocurrent generated on a carotenoid-sensitized TiO_2 nanocrystalline mesoporous electrode. J Photochem Photobiol A. 2000;130:49–56.
[10] Hao S, Jihuai W, Huang Y, Lin J. Natural dyes as photosensitizers for dye-sensitized solar cell. Solar Energy. 2006;80:209–214.
[11] Monishka RN. Review: Dye sensitized solar cells based on natural photosensitizers. Renewable Sustainable Energy Rev. 2012;16:208–215.
[12] Hug H, Bader M, Mair P, Glatzel T. Biophotovoltaics: Natural pigments in dye-sensitized solar cells. Appl Energy. 2014;115:216–225.
[13] Calogero G, Yum J-H, Sinopoli A, Di Marco G, Gratzel M, Nazeeruddin MK. Anthocyanins and betalains as light-harvesting pigments for dye-sensitized solar cells. Solar Energy. 2012;86:1563–1575.
[14] Alhamed M, Issa AS, Doubal WA. Studying of natural dyes properties as photo-sensitizer for dye sensitized solar cells (DSSC). J Electron Devices. 2012;16:1370–1383.
[15] Suhaimi S, Shahimin MM, Mohamad IS, Norizan MN. Comparative study of natural anthocyanins compound as photovoltaic sensitizer. Adv Environ Biol. 2013;7:3617–3620.

[16] Feng J, Jiao Y, Ma W, Nazeeruddin MK, GräTzel M, Meng S. First principles design of dye molecules with ullazine donor for dye sensitized solar cells. J Phys Chem C. 2013;117 3772—3778.
[17] Zhang J, Yh K, Hb L, Geng Y, Wu Y, Ya D, et al. Cyano or o-nitrophenyl? Which is the optimal electron-withdrawing group for the acrylic acid acceptor of D-π-A sensitizers in DSSCs? A density functional evaluation. J Mol Model. 2013;19:1597–1604.
[18] O'Regan B, Gratzel M. A low-cost, high-efficiency solar cell based on dye-sensitized colloidal TiO_2 Sfilms. Nature. 1991;353:737–740.
[19] Abdullah MI, Janjua MR, Mahmood A, Ali S, Ali M. Quantum chemical designing of efficient sensitizers for dye sensitized solar cells. Bull Korean Chem Soc. 2013;34:2093–2098.
[20] Schmidt MW, Baldridge KK, Boatz A. GAMESS. J Comput Chem. 1993;14:1347.
[21] Natalia M, Troisi A. Theoretical studies of dye-sensitised solar cells: From electronic structure to elementary processes. Energy Environ Sci. 2011;4:4473–4495 .
[22] Zhang J, Kan Y-H, Hai-Bin L, Geng Y, Yong W, Zhong-Min S. How to design proper p -spacer order of the DA dyes for DSSCs? A density functional response. Dyes Pigm. 2012;95:313–321.
[23] Delley B. From molecules to solids with the DMol^3 approach. J Chem Phys. 2000;113:7756.
[24] Koch R, Lipton AS, Slawomir F, Renugopalakrishnan V. Arginine interactions with anatase TiO_2 (100) surface and the perturbation of 49Ti NMR chemical shifts–a DFT investigation: Relevance to Renu-Seeram bio solar cell. J Mol Model. 2011;17:1467–1472.
[25] Greeves N. ChemTube3D. http://www.chemtube3d.com/index.html.
[26] Srinivas K, Kumar CR, Reddy MA, Bhanuprakash K, Rao VJ, Giribabu L. A-D organic dyes with carbazole as donor for dye-sensitized solar cells. Synth Met. 2011;161:96–105.
[27] Chang YJ, Chow TJ. Dye-sensitized solar cell utilizing organic dyes containing triarylene conjugates. Tetrahedron. 2009;65:4726.
[28] Kulhánek J, Bureš F. Imidazole as a parent π-conjugated backbone in charge-transfer chromophores. Beilstein J Org Chem. 2012;8:25–49.
[29] El Kouari Y, Migalska-Zalas A, Arof AK, Sahraoui B. Computations of absorption spectra and nonlinear optical properties of molecules based on anthocyanidin structure. Opt Quant Electron. 2015;47:1091–1099.
[30] Eka CP, Yuliarto B, Dipojono HK, Dipojono S. Theoretical investigation of anthocyanidin aglycones as photosensitizers for dye-sensitized TiO_2 solar cells. Adv Mater Res. 2015;1112:317–320.
[31] Duncan RW, Oleg VP. Theoretical studies of photoinduced electron transfer in dye-sensitized TiO_2. Annu Rev Phys Chem. 2007;58:84–143.
[32] Zhang G, Bala H, Cheng Y, Shi D, Lv X, Yu Q, et al. High efficiency and stable dye-sensitized solar cells with an organic chromophore featuring a binary π -conjugated spacer. Chem Commun 2009 2198—2200.
[33] Soto-Rojo R, Baldenebro-López J, Flores-Holguín N, Glossman-Mitnik D. Comparison of several protocols for the computational prediction of the maximum absorption wavelength of chrysanthemum. J Mol Model. 2014;20:2378.
[34] Preat J, Michaux C, Jacquemin D, Perpète EA. Enhanced efficiency of organic dye-sensitized solar cells: Triphenylamine derivatives. J Phys Chem C. 2009;113:16821–16833.
[35] Bourikas K, Kordulis C, Lycourghiotis A. Titanium dioxide (anatase and rutile): Surface chemistry, liquid-solid interface chemistry, and scientific synthesis of supported catalysts. Chem Rev. 2014;114:9754–9823.
[36] Burdett K, Hughbanks T, Miller GJ, Richardson JW, Smith JV. Structural-electronic relationships in inorganic solids: Powder neutron diffraction studies of the rutile and anatase polymorphs of titanium dioxide at 15 and 295 K. J Am Chem Soc. 1987;109:3639–3646.
[37] Henwood D, Carey JD. Molecular physisorption on graphene and carbon nanotubes: A comparative ab initio study. Mol Simul. 2008;34:1019–1023.
[38] Quartarolo AD, Russo N. A computational study (TDDFT and RICC2) of the electronic spectra of pyranoanthocyanins in the gas phase and solution. J Chem Theory Comput. 2011;7:1073–1081 .